Delft University of Technology

Hybrid Tunable Magnet Actuator

Design of a Linearized Force-Flux Tunable Magnet Actuator

Hoekwater, William B.; Ronaes, Endre; HosseinNia, Hassan

Important note
To cite this publication, please use the final published version (if applicable).
Please check the document version above.

Hybrid Tunable Magnet Actuator: Design of a Linearized Force–Flux Tunable Magnet Actuator

William B. Hoekwater, Endre Ronaes, and Hassan HosseinNia ⬮, *Senior Member, IEEE*

Abstract— **Recent studies have shown that tunable magnets (soft permanent magnets) can significantly reduce Joule heating in electromagnetic actuators. To achieve high motion accuracy and repeatability, this article proposes a novel actuator design with a linearized force–flux relation. In prior designs of variable reluctance tunable magnet actuators, the force and flux are related quadratically via a C-shaped actuator. Hybrid tunable magnet actuators based on biased fluxes are developed using lumped parameter models. Using finite element analysis, it is shown that the force–flux relation is symmetric linear around the mid position depending on the magnetic flux direction in the magnet. Within a position range of $\pm 500~\mu$m and a force range of ± 20 N, the linear fit produces a negligible error of 0.08 N. Finally, this linear relationship is validated with a 0.03-N error in an experimental setup.**

Index Terms—**Magnetic circuits, tunable magnets (TMs), variable reluctance actuator.**

I. Introduction

IN THE high-tech industry, thermal stability within motion and alignment systems is important to realize high accuracy and repeatability. However, coil-based actuators used in current systems will dissipate heat due to Joule heating. As a result, parts will start to deform and the position accuracy and repeatability of the machine will be destroyed [1]. For highly predictable linear motion actuators, Lorentz actuators are traditionally used because of their linear relation between force and current. However, these actuators have a poor efficiency due to the low force density and, thereby, is the position accuracy and repeatability limited [2]. In the past years, a reluctance actuator has been developed that has a ten times higher force density and, thereby, a higher efficiency [2]. Despite the higher efficiency, these actuators will still have Joule heating. This will especially lead to problems in quasi-static operations within vacuum environments where a force should be supplied for a longer time period. Examples of this type of systems are gravity compensators [3] and space mirror alignment systems [4].

In order to minimize the Joule heating in a quasi-static operation, prior research transformed reluctance actuators into hybrid reluctance actuators (HRA) using the permanent magnets (PMs) [5]. Besides this, the concept of in-situ magnetization adjustment of AlNiCo magnets was introduced in switchable electropermanent magnet (EPM) actuators [6]. In these actuators, an AlNiCo 5 magnet is placed in parallel with an NdFeB magnet, which are surrounded by a coil. By supplying a current pulse to the coil, the Netto magnetic flux is turned ON and OFF. As a result, the static magnetic flux is no longer created by coils but by magnets, and thereby, the heat dissipation is reduced.

Opposite to ON–OFF actuators, several in-situ magnetization adjustment actuators are developed that have a force range instead of only an ON–OFF state. A force tuning actuator for gravity compensation was developed by using a constant reluctance design [7]. To enable the implementation of in-situ magnetization adjustment for actuating applications, tuning algorithms for variable reluctance actuator designs are developed [8]. In this work, a C-shaped tunable magnet actuator (TMA) with an AlNiCo 5 magnet is used. With the saturation magnetization state tuning (SMST) method and control algorithms, which correct for the dynamics of the mover, the flux is tuned with 7 mT accuracy.

This research continues on the work done in [8], [9], and is part of a research program that investigates the application of in-situ magnetization tuning. The previous work done was focusing on developing flux tuning methods and flux control algorithms for a C-shaped actuator. Thereby, it neglects the nonlinear force–flux relation of a C-shaped magnetic actuator. This nonlinear force–flux relation will make it hard to use the actuator for high-precision motion or alignment systems where the force is controlled by linear controllers. Beside the problems in control, the nonlinear relations will result in an inefficient use of low fluxes. In contrast to the C-shaped actuator, this article investigates a linear TMA that generates a force proportional to the magnetic flux.

The contribution of this article is to design a topology of a TMA that has a linearized force–flux relation. This will improve the motion control of a TMA controlled by a linear controller and use the low fluxes more efficiently. To come up with a design of a linearized TMA, first, an analytical design is made with the use of lumped parameter models. The method of linearizing the force–flux relation in reluctance actuators by using biased fluxes [5] is used as the starting point. These biased reluctance actuators (HRA's) are used in high-precision motion and alignment systems, such as vibration isolation [10], gravity compensators [11], scanning motion systems [12], and
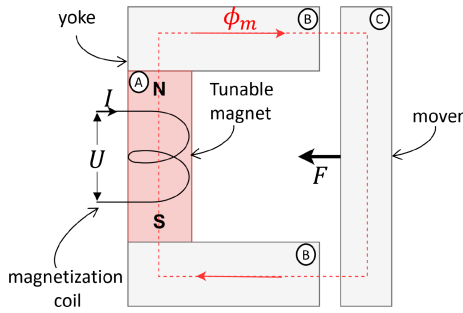
Fig. 1.　Schematic overview of the used C-shape actuator in [8], [9]. Part A: AlNiCo 5 magnet surrounded by a coil that is connected to a voltage source. Part B: the magnet is clamped between two ferromagnetic yoke parts. Part C: the mover is separated by two air gaps from the stator and closes the path of the magnetic flux ϕ_m.

mirror alignment systems [4]. Due to the different characteristics of tunable magnets (TMs) compared with iron yokes used in an HRA, a new electromagnetic circuit should be designed analytically that is optimized for TMs. The resulting actuator will be called a hybrid tunable magnet actuator (HTMA). This optimization is done with the use of a lumped parameter model. The analytically found linear relationship of the TMA is verified through finite element analysis (FEA), taking into account fringing fluxes. In addition, an experimental setup that incorporates manufacturing and material inaccuracies is used to validate the linear relationship.

The rest of this article is organized as follows. In Section II, the state of the art of a C-shaped TMA is shortly discussed based on [8], [9]. Second, Section III comes up with an analytical linearized TMA. This actuator is further studied using a COMSOL MULTIPHYSICS analysis discussed in Section IV. In Section V, the proposed linear relationship is validated by an experimental setup. Finally, Section VI concludes this article.

II. Working Principle of the TMA

In [8], [9], a C-shaped actuator, as shown in Fig. 1, is used. In this kind of actuator, the magnet is clamped between two ferromagnetic yokes. These yokes are separated by an air gap from the mover, and thereby, an attractive force is generated between the stator and the mover. An expression of the force can be found by using the Maxwell stress tensor [13] and can be simplified for the C-shaped actuator to

$$\boldsymbol{F} = \frac{1}{2\mu_0} \oint B_n^2 \boldsymbol{n} ds = \frac{B_g^2 A_g}{\mu_0} \tag{1}$$

where B_n is the magnetic flux density perpendicular to the yoke area and $\boldsymbol{n}$ is the outward normal vector. By using the hysteresis of the magnet and shift in load line by a current, it is possible to tune the magnet flux density B_g.

The load line defines the relation between the applied current and magnetic flux density inside the magnet as a result of the connected load to the magnet. For the C-shape actuator, it is defined as

$$B_m = -\mu_0 \frac{A_g l_m}{2 A_m l_g} \left(H_m - \frac{NI}{l_m} \right) \tag{2}$$

where A_g is the area of the yoke, l_m is the length of the magnet, A_m is the cross section of the magnet, l_g is the gap length, H_m is the applied field inside the magnet, N is the number of coil windings, and I is the applied current. When a voltage supply is used to create a current inside the coil, the voltage U is related to the flux density B_m as

$$U = IR + A_m N \frac{dB_m}{dt} \tag{3}$$

where R is the resistance of the coil.

The SMST method used for in-situ magnetization state tuning can be graphically described, as shown in Fig. 2. The method consists of four steps that should be followed to magnetize a magnet to a desired magnetization level. Important to notice is the squared relation between the applied force and the magnetic flux density in the magnet, as shown in (1). This will result in inaccurate control if the system is motion controlled by linear controllers.

III. Hybrid TMA

The problem of the nonlinear force–flux relation of C-shaped reluctance actuators is solved by introducing the HRA concept [12], [14], [5]. This kind of actuator uses a bias flux ϕ_{pm} that is generated by a PM and a control flux that is generated by coils. Due to the opposite directions of the biased flux relative to the control flux in the gaps, a linear force–flux relation is obtained. This principle of linearizing is summarized by the schematic shown in Fig. 3.

The design requirement for a linearized force–flux TMA can be simplified to the requirement that the flux paths of the biased flux and the control flux shown in Fig. 3 should be closed by PMs and tunable magnets. This means that the green and blue flux lines shown in the top part should be closed by using PMs and TMs, respectively. Some important rules should be taken into account while closing the flux lines.

1) The flux of the TM should not go through the PM. Due to the high reluctance of the PM, the TM will be used inefficiently. Also, the flux of the TM should not be shortcutted by iron yokes. If it is shortcutted by the iron yoke, no flux will flow through the mover and, thereby, no force will be generated. The TM will act as a barrier for other fluxes if the length is larger than the gap lengths.
2) The flux of the PM should not go through the TM and should not be interrupted by an iron yoke. Also, the PM will act as a barrier for the other fluxes if the length is larger than the gap lengths.

Directly replacing the coils of the HRA by TMs will not fulfill the general requirement rules of closing the flux paths due to the large reluctance of the TMs. Therefore, this actuator will be inefficient and unstable. After an iterative design process that is described in more detail in [15], the actuator of Fig. 4 is designed. In this actuator, the different parts are rearranged such that the flux of the PM through the TM is reduced. By using Maxwell
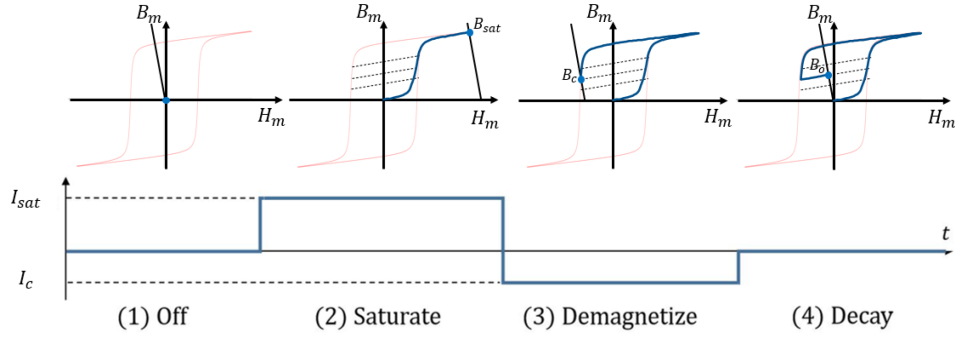
Fig. 2. Graphical representation of the SMST method. (1) Initial state in this case is the OFF or nonmagnetized state. (2) By applying a positive current, the load line will shift and the magnet will be saturated. (3) After applying a negative current, the load line will shift to the corner point. (4) By removing the current, the load line will shift back to the origin and the operation point will be reached.
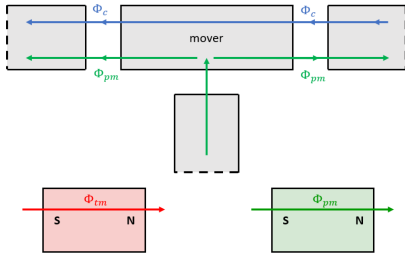

Fig. 3. Schematic representation of the linearization method, shown at the top. The fluxes are represented by arrowed lines. The gray blocks represent iron yoke material, where the dashed lines represent the location where other parts should be connected to close the flux lines. The flux lines through the mover should be closed by using the building blocks shown at the bottom: the left (red) block represents a TM, and the right (green) block represents a PM. Also, iron yokes can be used.

stress tensors, the force in this actuator can be described as

$$
F = \frac{(\phi_{\text{pm},gL} + \phi_{\text{tm}})^2 - (\phi_{\text{pm},gR} - \phi_{\text{tm}})^2}{2\mu_0 A_g}
$$

$$
\approx \frac{2\phi_{\text{pm}}}{\mu_0 A_g}\left(\phi_{\text{tm}} + \phi_{\text{pm}}\frac{2x}{2l_g + \mu_0 A_g \mathcal{R}_{\text{tm}}}\right) \quad (4)
$$

where ϕ_{tm} is the control flux generated by the TM. The flux of the PM in the gaps, $\phi_{\text{pm},gL}$ and $\phi_{\text{pm},gR}$, can be expressed as a function of the flux in the two PMs ϕ_{pm}, the reluctance of the TM $\mathcal{R}_{\text{tm}}$ and the position of the mover. The expression of the force, as shown in (4), can be simplified by defining a motor constant K_m and an actuator stiffness k_a to an expression that only depends on the control flux ϕ_{tm} and the position x

$$
F = K_m \phi_{\text{tm}} + k_a x. \quad (5)
$$

In order to derive the expressions for the fluxes, a lumped electromagnetic model is designed, see Fig. 4. For this model, it is assumed that the relative permeability of the yokes is sufficiently large to neglect the reluctance of these components. The reluctance of the left gap $\mathcal{R}_{g,L}$, right gap $\mathcal{R}_{g,R}$, fixed gap $\mathcal{R}_f$, PMs $\mathcal{R}_{\text{pm}}$, and TM $\mathcal{R}_{\text{tm}}$ can be expressed as

$$
\mathcal{R}_{g,L} = \frac{l_g - x}{\mu_0 A_g}, \mathcal{R}_{g,R} = \frac{l_g + x}{\mu_0 A_g}, \mathcal{R}_f = \frac{l_f}{\mu_0 A_g}
$$

$$
\mathcal{R}_{\text{pm}} = \frac{l_{\text{pm}}}{\mu_0 A_{\text{pm}}}, \mathcal{R}_{\text{tm}} = \frac{l_{\text{tm}}}{\mu_0 \mu_r A_{\text{tm}}} \quad (6)
$$

where x is the position of the mover, l_f is the length of the gap between the yoke in the middle and the mover, l_{tm} is the length of the TM, and l_{pm} is the length of the PMs. The areas of the gaps are all fixed to the same size A_g, and the areas of the TM and PM are A_{tm} and A_{pm}, respectively. μ_r is the relative permeability of the TM and will change based on the BH-curve of AlNiCo 5.

By using superposition, the model can be split up into two parts: the magnetic flux generated by the TM and the magnetic flux generated by the PMs. Ideally, due to the fact that the PM behaves as an air gap, no flux of the TM is flowing through the PM as long as $l_{\text{pm}} \gg l_g$. Therefore, the flux ϕ_{tm} in the TM without losses can be described, as shown in (7). The flux of the TM in the air gaps is equal to the flux in the TM and independent of the position x

$$
\phi_{\text{tm}} = \phi_{\text{tm},L} = \phi_{\text{tm},R} \approx \frac{k_{mmf} H_{\text{tm}} l_{\text{tm}}}{k_L \mathcal{R}_{g,L} + k_R \mathcal{R}_{g,R}} \quad (7)
$$

where H_{tm} is the applied magnetic field of the TM, k_L and k_R are loss factors for fluxes, and k_{mmf} is a loss factor for the magnetomotive force

$$
k_L = \frac{\phi_{\text{tm},L}}{\phi_{\text{tm}}} = \frac{B_{\text{tm},L} A_g}{B_{\text{tm}} A_{\text{tm}}}, k_R = \frac{\phi_{\text{tm},R}}{\phi_{\text{tm}}} = \frac{B_{\text{tm},R} A_g}{B_{\text{tm}} A_{\text{tm}}} \quad (8)
$$

$$
k_{mmf} = \frac{H_L(l_g - x) + H_R(l_g + x)}{H_{\text{tm}} l_{\text{tm}}}. \quad (9)
$$

H_L and H_R are the magnetic field strengths in the left and right gaps, respectively. By using (7), the flux inside the TM as a result of the TM part can be found as

$$
B_{\text{tm}} = -\frac{k_{mmf}\mu_0 A_g l_{\text{tm}}}{((k_L + k_R)l_g + (k_R - k_L)x)A_{\text{tm}}}\left(H_{\text{tm}} - \frac{NI}{l_{\text{tm}}}\right). \quad (10)
$$

This equation is called the load line that defines the magnetic flux inside the magnet and the applied field to the magnet based on the circuit load.

The circuit of the PMs depends on the properties of the PM, TM, and the gaps. However, if l_{pm} is way larger than l_f and l_g, the flux in each PM can roughly be estimated by taking only the PM reluctance into account. By using superposition of the two
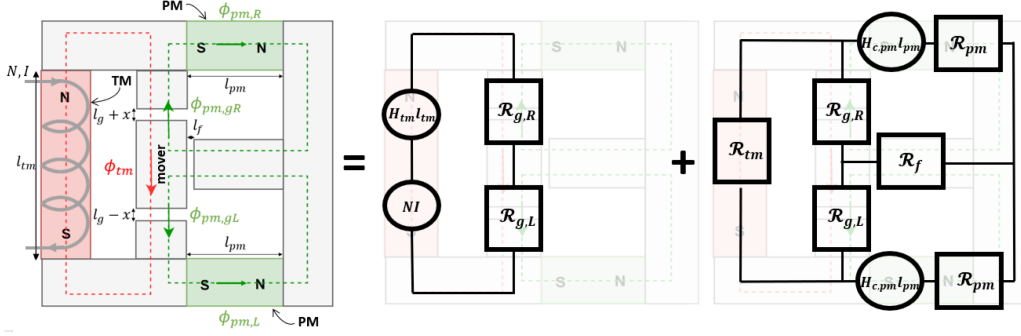
Fig. 4.   Schematic overview of the linearized HTMA (left schematic). The bias flux is delivered by two PMs whose main flux paths are shown by dashed lines. The control flux is delivered by the TM which main flux path is shown by a dashed line. By using superposition, two lumped electromagnetic circuits can be drawn. The flux of the TM will only flow through the gaps (mid schematic). The flux of the PMs will both flow through the gaps and the TM (right schematic).

PMs, the PM flux in the gaps can be expressed as follows:

$$\phi_{\mathrm{pm},gL} \approx \frac{2l_g + 2x + \mu_0 A_g \mathcal{R}_{\mathrm{tm}}}{2l_g + \mu_0 A_g \mathcal{R}_{\mathrm{tm}}} \frac{H_{c,\mathrm{pm}} L_{\mathrm{pm}}}{\mathcal{R}_{\mathrm{pm}}}$$

$$\phi_{\mathrm{pm},gR} \approx \frac{2l_g - 2x + \mu_0 A_g \mathcal{R}_{\mathrm{tm}}}{2l_g + \mu_0 A_g \mathcal{R}_{\mathrm{tm}}} \frac{H_{c,\mathrm{pm}} L_{\mathrm{pm}}}{\mathcal{R}_{\mathrm{pm}}} \quad (11)$$

where $H_{c,\mathrm{pm}}$ is the coercivity of the PM. It is important to notice that the flux in (11) depends on the reluctance of the TM. This reluctance depends on the relative permeability of the AlNiCo 5 magnet, which changes while tuning (between 5 and 270 depending on the position in the BH-curve [16]). In addition to the influence of the TM on the PM flux, the PM will also influence the load line of the TM. By using superposition of the two PMs, the load line of the PM circuit to the TM can be described as

$$B_{\mathrm{tm}} = -\frac{2\mu_0 A_g l_{\mathrm{tm}}}{A_{\mathrm{tm}}} G_{\mathrm{pm}} \left(H_{\mathrm{tm}} - \frac{H_{c,\mathrm{pm}} l_{\mathrm{pm}}}{l_{\mathrm{tm}}} \right) \quad (12)$$

where

$$G_{\mathrm{pm}} = \frac{k_{\mathrm{pm}} x}{\left(l_g^2 - x^2 + 2\mu_0 l_g A_g \left(\mathcal{R}_f + \mathcal{R}_{\mathrm{pm}} \right) \right)}. \quad (13)$$

k_{pm} is a loss factor to correct for losses in both magnetomotive forces and fluxes. The PMs will apply a magnetic field to the TM, which will result for offset positions of the mover in a shift, like in the case of the current in (10). Due to the fact that the applied magnetic fields of the two PMs are opposite in the TM, there will be no influence on the load line in the mid position ($x = 0$). The total load line of the circuit is the summation of (10) and (12)

$$B_{\mathrm{tm}} = K_{\mathrm{load}} H_{\mathrm{tm}} + \Delta_{\mathrm{load}} + \Delta_I \quad (14)$$

where $K_{\mathrm{load}} = -\frac{\mu_0 A_g l_{\mathrm{tm}}}{A_{\mathrm{tm}}} \left(\frac{k_{mmf}}{(k_L + k_R)l_g + (k_R - k_L)x} + 2G_{\mathrm{pm}} \right)$,
$\Delta_{\mathrm{load}} = \frac{2\mu_0 A_g l_{\mathrm{tm}}}{A_{\mathrm{tm}}} G_{\mathrm{pm}} \frac{H_{c,\mathrm{pm}} l_{\mathrm{pm}}}{l_{\mathrm{tm}}}$ and $\Delta_I = NI$
$\frac{k_{mmf} \mu_0 A_g}{((k_L + k_R)l_g + (k_R - k_L)x)A_{\mathrm{tm}}}$.

The loss factors included in the load line, the motor constant, and actuator stiffness will be determined using an FEA in the following section.
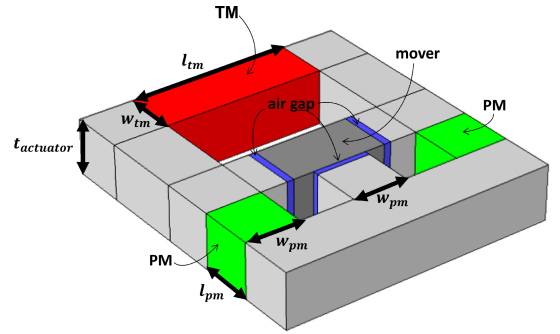

Fig. 5.   COMSOL model of the simple HTMA used for loss factor studies depending on the dimensions of the actuator.

IV. IDENTIFYING THE LOSS 3-D FEM ANALYSIS

To study the behavior of the HTMA and identify losses, a COMSOL MULTIPHYSICS simulation is performed. With the use of this simulation, both the flux losses and magnetomotive force losses can be estimated. These losses are geometry dependent and influence the tuning and performance of the actuator, but will not change the linearity of the actuator. To come up with some rules of thumb for optimizing the dimensions of an HTMA in future work, the losses and performance of the actuator for different magnet dimensions are studied. Fig. 5 shows the geometry of the actuator with a constant thickness of t_{actuator}. The lengths l_{pm} and l_{tm} and widths w_{pm} and w_{tm} of the PM and the TM are used as independent variables. These dimensions influence the slope K_{load} and shift Δ_{load} of the load line that is used for tuning the actuator, see Fig. 6. A larger slope of the load line results in a larger range of remanent magnetic fluxes. From (14) it is obvious that an offset position of the mover will cause a shift in the load line because of the actuator's asymmetric behavior. The smaller the shift is, the more robust the actuator will be against position disturbances.

The performance of the actuator is described by the force F that it can generate and the amount of energy, E_{tune}, it costs to tune the magnet. The results of the COMSOL analysis are listed in Table. I. A few general remarks can be made based on this analysis.
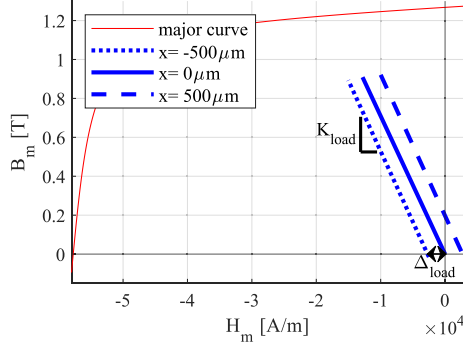
Fig. 6. Load lines for three different positions for an actuator with $I = 0$, $l_{\mathrm{tm}} = 30$ mm, and $t_{\mathrm{actuator}} = 10$ mm (t_{actuator} is the thickness of the actuator). Placing the mover outside the mid position will result in a negative or positive shift in load line.

TABLE I
SUMMARY OF THE INFLUENCE OF THE MAGNET DIMENSIONS ON THE ACTUATOR BEHAVIOR

	k_{load}	Δ_{load}	F	E_{tune}
l_{tm}	↑	↓	↑	↑
w_{tm}	↓	↓	↑	↑
t_{actuator}	↓	↑	↑	↑
l_{pm}	↓	↑	↑	-
w_{pm}	↑	↑	↑	-

↑ Means that the performance increases with increasing dimensions, whereas ↓ means decreasing performance. Red marked arrows indicate that by increasing the dimensions, the performance will decrease. Black arrows indicate that by increasing the dimensions, the performance will increase.

1) The PMs will apply a shift to the load line. The shift depends on the reluctance of the TM and the position of the mover that can result in a less robust or inefficient actuator.
2) Flat magnets will result in higher actuator performance, both in terms of force and energy. To make an actuator with high performance and stability, the right combination of the width and length of the magnet should be selected.

The HTMA can be reshaped in a folded 3-D configuration, see Fig. 7, which will improve the compactness of the actuator. In this actuator, a cylindrical TM is used due to time limitations and the available in-stock magnets in the lab. The shape of the magnets does not influence the linear force–flux relationship. COMSOL simulations are used to identify the behavior of this actuator, which is also used in the experimental setup, as will be described in Section V. To show the linear relation between the force and magnetic flux in the TM, the force for different remanent flux densities and positions of the mover is calculated, see Fig. 8(a). To calculate the motor constant K_m, introduced in (4), the force is linearized as a function of the flux for different positions. The forces around the mid position of the mover are a linear function of the magnetic flux, whereas forces further away from the mid position become slightly nonlinear with respect to the flux. By identifying the model, it can be observed
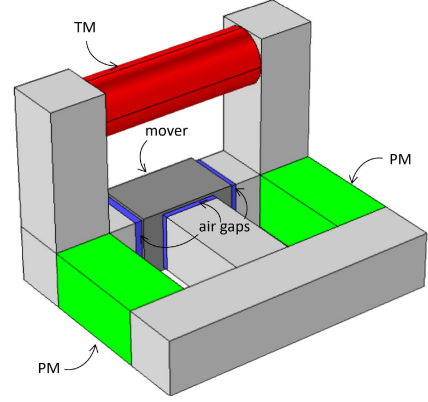

Fig. 7. Schematic overview of the 3-D folded HTMA. The TM is shown in red, the PMs in green, the mover in dark gray, the stator in gray, and the air gaps in blue.

that this nonlinearity is symmetric around the mid position for positive and negative fluxes. Thus, $K_m(x)$ can be approximated by a fourth order polynomial which is mirrored for positive and negative fluxes; For positive fluxes, $K_m(x)$ should be used and for negative fluxes $K_m(-x)$ should be used resulting in:

$$K_m(x) \approx \begin{cases} 2 \cdot 10^{16}x^4 - 1.28 \cdot 10^{13}x^3 \\ +9.53 \cdot 10^{10}x^2 - 3.00 \cdot 10^7 x \\ +1.55 \cdot 10^5 & \phi_{\mathrm{tm}} < 0 \\ 2 \cdot 10^{16}x^4 + 1.28 \cdot 10^{13}x^3 \\ +9.53 \cdot 10^{10}x^2 + 3.00 \cdot 10^7 x \\ +1.55 \cdot 10^5. & \phi_{\mathrm{tm}} > 0 \end{cases} \quad (15)$$

The offset of the linearized force relation is used to estimate the actuator stiffness k_a as follows:

$$k_a(x) \approx 4.67 \cdot 10^9 x^2 + 1.54 \cdot 10^5 x + 8.71 \cdot 10^3. \quad (16)$$

Fig. 8(b) shows a graphical representation of the model constants. The method for finding the actuator constants assumes a linear fit of the force–flux relation and a third-order fit for the force offset in the mid position. The root-mean-squared error (RMSE) introduced by using this linearized model is approximately 0.08 N, which shows that the nonlinearities in the modeled position range can be neglected.

Based on the stiffness, it is observed that the HTMA is a negative stiffness actuator, and thereby, the actuator itself is unstable. In order to create a stable system, a parallel leaf spring flexure can be connected to the mover. By using the flexure properties, as listed in Table II, a flexure stiffness of 11.8 kN/m is obtained, which results in a total positive stiffness, as shown in Fig. 8(c).

For the tuning of the magnet, it is important to determine the shift Δ_{load} and slope k_{load} of the load line. Based on COMSOL simulations, the offset of the load line as a function of the position can be directly approximated by the linear equation

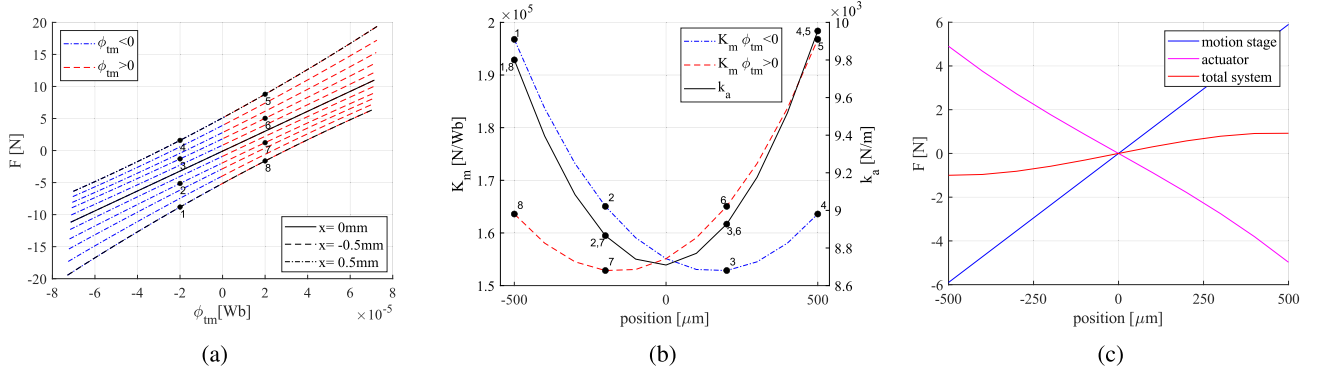$$\Delta_{\mathrm{load}}(x) = 5.35 \cdot 10^6 x - 2.67. \quad (17)$$

Fig. 8. COMSOL results of the (a) forces, (b) motor constant, and actuator stiffness and (c) stiffness forces of the system. Positive fluxes mean fluxes to the left through the gap. Data points 1–8 are added to give a better insight in the relation between (a) and (b).

TABLE II
PARAMETERS USED IN THE COMSOL SIMULATION OF THE FOLDED HTMA

Symbol	Value	Quantity	Source
AlNiCo 5 magnet (LNG 44)			
l_{tm}	30 mm	Magnet length	[17]
d_{tm}	10 mm	Magnet diameter	[17]
$B_{r,tm}$	1.25 T	Remanent flux density	[17]
$H_{c,tm}$	50 kAm^{-1}	Coercive force	[17]
$H_{sat,tm}$	150 kAm^{-1}	Saturation field intensity	
$\mu_{r,max}$	270	Max relative permeability	[9]
μ	$0.95B_{r,tm}$+4.96	Relative permeability recoil lines	[9]
τ	0.126 ms	Magnetic diffusion time saturation	[18]
NdFeBr magnet (N48)			
l_{pm}	20 mm	Magnet length	[19]
w_{pm}	10 mm	Magnet width and height	[19]
$B_{r,pm}$	1.38 T	Remanent flux density	[19]
$\mu_{r,pm}$	1.05	Relative permeability	[19]
Magnetic circuit (electrical steel)			
$\mu_{r,es}$	4000	Relative permeability	
A_g	100 mm^2	Air gap surface area	
l_g	1.25 mm	Length air gap mid position	
l_f	1 mm	Length fixed air gap	
Parallel leaf spring			
l_{fl}	28 mm	Length of a flexure	
w_{fl}	12.7 mm	Width of a flexure	
t_{fl}	0.3 mm	Thickness of a flexure	
n_{fl}	4	Number of flexures	
E_{st}	200 GPa	Young's modulus spring steel	

Fig. 9. Comparison of the C-shaped TMA and the HTMA based on COMSOL results.

For calculating the slope of the load line, the loss factors are identified based on the COMSOL model as follows:

$$k_L(x) = 2.15 \cdot 10^{10} x^4 + 2.93 \cdot 10^7 x^3$$
$$+ 5.61 \cdot 10^4 x^2 + 98.9x + 0.266 \quad (18)$$

$$k_R(x) = 2.15 \cdot 10^{10} x^4 - 2.93 \cdot 10^7 x^3$$
$$+ 5.61 \cdot 10^4 x^2 - 98.9x + 0.266 \quad (19)$$

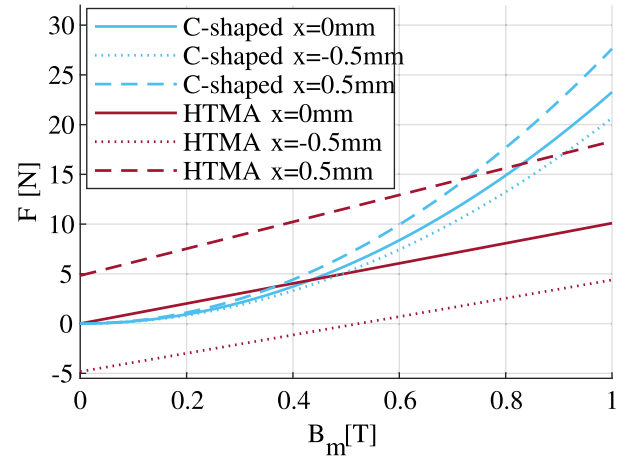$$k_{mmf}(x) = -2.59 \cdot 10^3 x^2 - 16 \cdot 10^{-4} x + 0.982 \quad (20)$$

Notice that k_L and k_R are symmetric around the mid position. The error introduced by using the loss factors to calculate the slope of the load line by using (10) is approximately 15.5 nTm/A, which is negligible compared to a load line slope of 72.6 mTm/A. Based on the COMSOL simulations it is proven that it is possible to create an overall stable actuator that has a linear force–flux relation. Fig. 9 shows the force of both the designed HTMA and the C-shaped actuator designed in [9]. The force–flux relation of the HTMA is linear compared with the quadratic relation of the C-shaped version. The parameters used for the C-shaped actuator are listed in Table III. Thereby, it is proven that the designed topology is suitable to linearize the C-shaped actuator. However, the amplitude of the force decreased and the position dependence of the force increased. In the next section, an experimental setup of this actuator is built to validate this linear relationship.

V. EXPERIMENTAL SETUP

The folded version of the HTMA is converted into an experimental setup, as shown in Figs. 10 and 11. An AlNiCo 5 cylindrical magnet is used for the control flux. The biased flux

TABLE III
PARAMETERS USED FOR THE C-SHAPED ACTUATOR

| Symbol	Value	Quantity	Source
AlNiCo 5 magnet (LNG 44)			
l_{tm}	30 mm	Magnet length	[17]
d_{tm}	10 mm	Magnet diameter	[17]
$B_{r,tm}$	1.25 T	Remanent flux density	[17]
$H_{c,tm}$	50 kAm^{-1}	Coercive force	[17]
$H_{sat,tm}$	150 kAm^{-1}	Saturation field intensity	
$\mu_{r,max}$	270	Max relative permeability	[9]
μ_r	$0.95B_{r,tm}$+4.96	Relative permeability recoil lines	[9]
τ	0.126 ms	Magnetic diffusion time saturation	[18]
Magnetic circuit (electrical steel)			
$\mu_{r,es}$	4000	Relative permeability	
A_g	100 mm^2	Air gap surface area	
l	1.25 mm	Length air gap mid position	
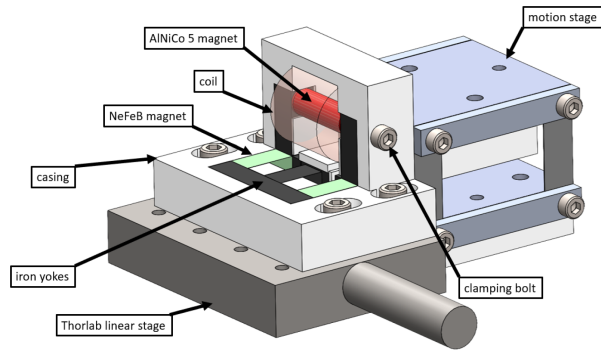
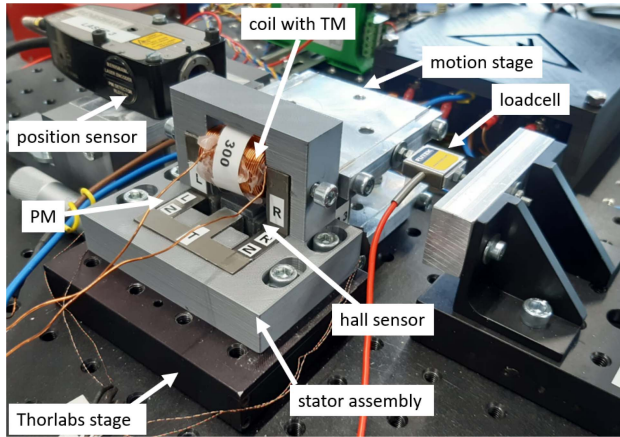Fig. 10. CAD model of the experimental setup.

Fig. 11. Experimental setup.

is delivered by two neodymium magnets, NdFeBr N48, and the yoke is created out of laminated electrical steel. The mover of the actuator is connected to a compliant linear motion stage. This stage is designed in such a way that the whole actuator has a small positive stiffness behavior in the range of -500 to 500 μm. The position of the mover is measured with a resolution of 39.5 nm using a Renishaw RLD10 differential interferometer. The coil around the TM has 300 windings and is created out

TABLE IV
EXPERIMENTAL STIFFNESSES OF THE DIFFERENT PARTS OF THE ACTUATOR

	Stiffness (kN/m)	RMSE (mN)	3σ (N/m)
mover	12	10	21
actuator	-4.4	45	20
total system	7.6	45	20

of 0.75-mm thick copper wire. This coil is connected to an H-bridge created out of four Sensata/Crydom 20 A Solid-State Relays and powered by a Delta SM 52-AR-60 power supply. This power supply delivers 52 V and is used in current control mode. The current is measured by a Polulu ACS714 ±30 A current sensor. To measure the flux in the gaps, two Asensor Technology HE144 Hall sensors are used, which are placed in brackets with a thickness of 0.75 mm. These brackets are clamped around the stator poles. The required input current of 1 mA of the Hall sensors is delivered by a custom-made precision current pump that makes use of two opamps. A custom-made signal condition board as used in [9] amplifies the Hall sensor signals and low-pass filters them at 3 kHz. To measure the force of the actuator, an FLLSB200 S-BEAM Junior 45-N loadcell is connected between the mover and a Thorlabs manual linear motion stage. A CompactRIO, NI c-RIO 9039, is used to log the sensor data at 10 kHz. With the use of NI LabView software, the same CompactRIO takes care of the output control signals for tuning the TM.

For this experimental setup, the stiffness of the motion stage, the passive stiffness of the actuator, and the force on the mover for different remanent fluxes in the TM are measured. The stiffness of the motion stage can be determined by measuring the force at different positions without a connected stator. The resulting force position graph is shown in Fig. 12(c) (motion stage line). The stiffness of the flexures is estimated with a 3σ repeatability of 21 N/m to be 12 kN/m. The linear fit used for this estimation has an RMSE of 0.01 N. The stiffness of the total system can be measured by adding the stator with demagnetized TM to the motion stage. The total system stiffness (total system line) is estimated with the use of a linear fit as 7.6 kN/m with an RMSE of 0.045 N and a 3σ repeatability of 20 N/m. Due to the misalignment of the stator with respect to the mover, the force will be nonzero in the mid position. The misalignment is caused by manufacturing tolerances of the yokes and assembly tolerances of the Hall sensors. Based on PM flux measurements, a position correction of -119 μm is used for the actuator position. This correction is applied in the force–position plot of Fig. 12(c), and thereby, the used position scale is calibrated with respect to the stator. However, due to this correction, the force of the motion stage will not be zero in the mid position of the stator.

The stiffness of the actuator (actuator line) can be calculated based on the stiffness of the motion stage and the stiffness of the system. By using a linear fit, the actuator stiffness is estimated as -4.4 kN/m with an RMSE of 0.045 N and a 3σ repeatability of 20 N/m. The different stiffnesses are summarized in Table IV.
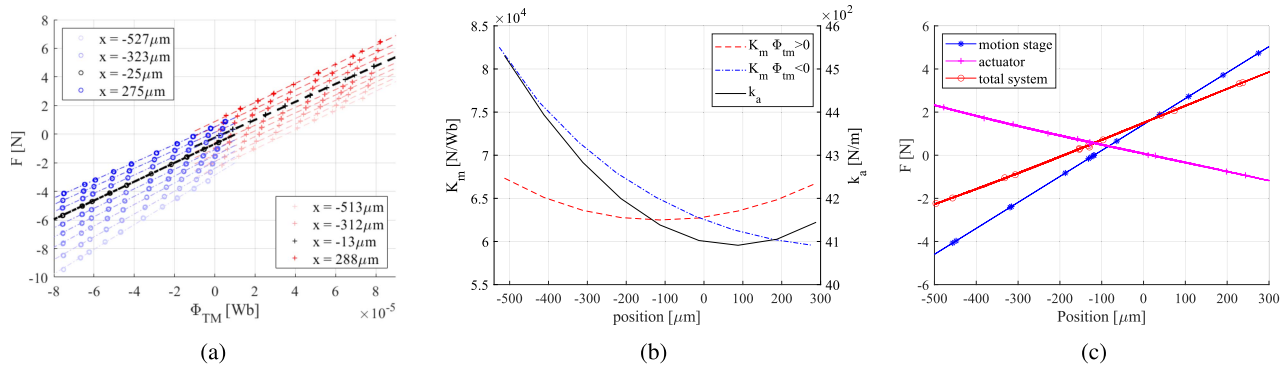
Fig. 12. Experimental results of the (a) forces, (b) motor constant, and actuator stiffness and (c) stiffness forces of the system. Positive fluxes mean fluxes to the left through the gap. The fluxes in the magnet are estimated based on the right gap sensor.

TABLE V
REPEATABILITY AND ACCURACY OF THE EXPERIMENTAL RESULTS FOR THE MOTOR CONSTANT ESTIMATION

	Repeatability 3σ	Accuracy
F	51 mN	± 0.1 N
position	0.25 μm	± 10 μm
Φ_{tm}	0.38 μWb	± 4 μWb
K_m	22 N/wb	

To validate the linear force–flux relation in the experimental setup, the TM is tuned with the SMST method at nine different positions to ten remanent magnetic fluxes both for positive and negative directions.

For each of these remanent fluxes, the force and flux densities in the gaps are measured. For the quantities needed to show the linearity between the force and flux, the repeatability and accuracy of the experimental values are given in Table V. By adding the flexure force to the measured loadcell force, the actuator force can be calculated. This force is determined with a 3σ repeatability of 51 mN. The loadcell that is used needs deformation to measure forces. These deformations will result in maximum position changes of 20 μm, which will result in a force accuracy of ± 0.1 N.

To estimate the flux in the TM, first, the flux of the TM in the gaps is calculated by subtracting the PM fluxes estimated in the demagnetized setup from the measured gap fluxes. Second, the flux density inside the TM is estimated by using (8) and the calculated TM gap flux densities. The values of the flux losses found by the COMSOL simulation are corrected by a constant factor of 0.71. This correction factor is determined by fitting the remanent flux density of major loop measurements to the theoretical remanent flux density of AlNiCo 5. The steady-state magnetic flux densities in the TM can be estimated with a 3σ repeatability of 0.38 μWb. However, the model accuracy of this estimation is in the order of ± 4 μWb. The accuracy is estimated by using the difference between the estimated flux in the TM based on the left and right gaps. This difference is the result of manufacturing and alignment tolerances, which are in the

range of 100 μm. These tolerances can lead to an asymmetric actuator, and as a result, the real position and flux losses will differ from the estimated ones. As a result, the estimated fluxes in the TM based on the left and right gaps will not be the same. This inaccuracy of the model will not influence the motion control accuracy if both the actuator model and the TM model are identified based on the fluxes in one of the gaps.

The results of the measurements are shown graphically in Fig. 12(a). For the different positions, a linear line is fitted through the data. Based on this fit, the motor constant and the stiffness can be determined, as shown in Fig. 12(b). The motor constant is determined with a 3σ repeatability of 22 N/Wb.

When comparing the behavior of the experimental setup with the COMSOL simulation, differences in both the slope and the offset of the force–flux plot can be observed. These deviations are likely caused by dimensional differences between the simulated model and the test setup, resulting from manufacturing errors, and magnetic imperfections in the PM material.

In the experimental setup, a 0.8 times lower PM flux compared with the FEA is measured. This difference can be explained by extra fringing losses due to the tolerances of the manufacturing procedures and of the magnetic properties of the constituent parts. Based on (11), it is observed that variations in both relative permeability and coercivity of the magnets influence the magnetic flux density in the air gaps. The flux contribution from the TM may also have been lowered as a result of fringing or manufacturing errors, such as, but not limited to, different air gap lengths, a difference in the area of the pole surfaces at opposite sides of the air gaps and nonparallel surfaces affecting the air-gap reluctances and loss factors in (7). For verification, further FE simulations were performed considering the actual dimensions of the fabricated actuator alongside a range of possible factors causing it to underperform, including a lower remnant magnetization state of the NdFeB magnets than anticipated, air gaps between the assembled parts, and an angular misalignment of opposing pole surfaces. Fig. 13(a) illustrates the force–flux relation of the simulated model with a combination of the aforementioned features that results in a similar behavior to that which was measured from the lab-setup (see Fig. 12). An offset in the force–displacement relation of the system illustrated in Fig. 8(c) also results from the equilibrium of
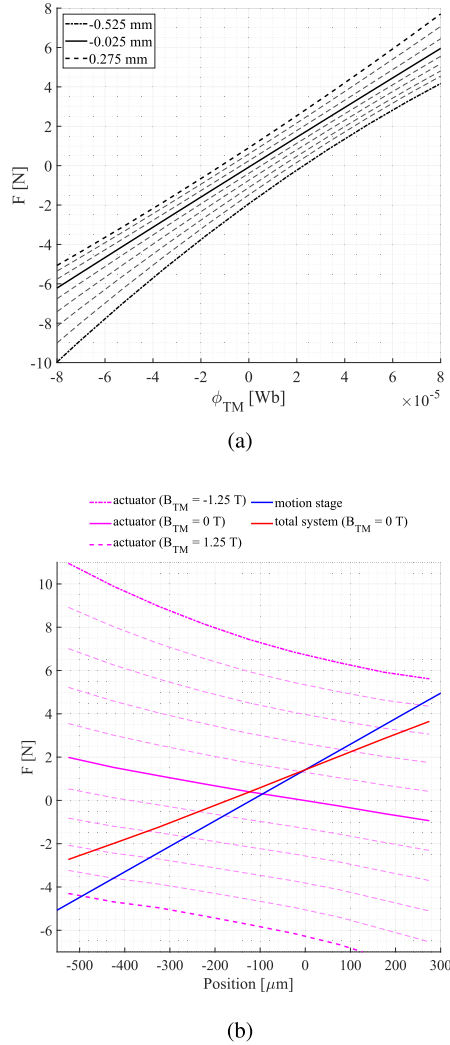
(a)

(b)

Fig. 13. COMSOL results from a model with the measured dimensions of the manufactured setup, air gaps between assembled parts of $0.3\,\mathrm{mm}$, a reduction of the remnant magnetic flux of the NdFeB PMs of 20%, and nonparallel stator poles (with a deviation $0.45\,\mathrm{mm}$ in distance to the mover between the upper and lower edges). (a) Force–flux relation in the displacement range of the prototype. (b) Force–displacement behavior of the system with the spring mechanism having an offset equilibrium by $-120\,\mu\mathrm{m}$.

the spring mechanism being offset from that of the mover in the magnetic circuit. This offset is also factored into the simulated model to attain a similar force–displacement behavior, as shown in Fig. 13(b).

To improve the experimental setup such that it fits better with the simulation results, improvements should be made mainly to the manufacturing tolerances and alignment of the air gaps, and the clamping of the magnets [8]. Despite the model inaccuracy of the flux in the TM and the difference between the COMSOL model and the experimental setup, the averaged RMSE of the linear fit is around 0.03 N. This indicates that the designed TMA topology has a reliable linear force–flux relation. Inaccuracies in both FEA and experimental setup can lead to shifts or linear scaling of the force–flux relation, but will not affect the linearity of the actuator. Thereby, it is validated that the force–flux relation

of an HTMA for a range of -500 to 300 μm can be approximated by a linear fit.

VI. CONCLUSION

This article proposed an HTMA with a linearized force–flux relation such that motion control would be more accurate for linearized controllers. Lumped electromagnetic models revealed that the concept of using biased fluxes to linearize the force–flux relation could be used in an HTMA. The actuator should be constructed using two PMs and one TM, where the PMs provided a bias flux to the TM flux. At one side of the mover, this biased flux would add to the TM flux, whereas at the other side, the biased flux would subtract from the TM flux. A finite element-based model revealed the linearity around the mid position. By creating an experimental setup of the concept of the HTMA, it was validated that the force–flux relation was linear in the position range of -500 to 300 μm and TM flux range of -80 to 80 μWb.

Future work includes to develop motion control for the HTMA by identifying a magnetic model in the actuator and implementing current, flux, and position control algorithms. For the implementation of the flux control, the shift in the load line as a result of the position observed in the FEA in this research should be taken into account. Another direction of future work is to optimize an HTMA for other performance, such as the force density and efficiency of the actuator by changing the dimensions. In this way, an actuator can be obtained that can be used in a wider variety of applications.

REFERENCES

[1] E. Lomonova, "Advanced actuation systems-state of the art: Fundamental and applied research," in *Proc. Int. Conf. Elect. Mach. Syst.*, 2010, pp. 13–24.
[2] N. Vrijsen, J. Jansen, and E. Lomonova, "Comparison of linear voice coil and reluctance actuators for high-precision applications," in *Proc. IEEE 14th Int. Power Electron. Motion Control Conf.*, 2010, pp. S3–29.
[3] S. A. J. Hol et al., "Design and optimization of a magnetic gravity compensator," Ph.D. thesis, Technische Universiteit Eindhoven. [Online]. Available: https://doi.org/10.6100/IR574485
[4] S. Kuiper, N. Doelman, E. Nieuwkoop, T. Overtoom, T. Russchenberg, and M. e. a. van Riel, "Electromagnetic deformable mirror development at TNO," in *Proc. Adv. Opt. Mech. Technol. Telescopes Instrum. II*, 2016, pp. 24–30.
[5] R. M. Schmidt, G. Schitter, and A. Rankers, *The Design of High Performance Mechatronics: High-Tech Functionality by Multidisciplinary System Integration*, 3rd ed. Amsterdam, The Netherlands: Delft University Press, 2020.
[6] A. N. Knaian, "Electropermanent magnetic connectors and actuators: Devices and their application in programmable matter," Ph.D. dissertation, Massachusetts Inst. Technol., Cambridge, MA, USA, 2010.
[7] T. Hüfner, O. Radler, T. Ströhla, T. Sattel, J. Wesselingh, and A. E. A. Vogler, "A note on electromagnetic gravity compensation actuators based on soft electropermanent magnets for adjustable reluctance force," in *Proc. 17th Int. Conf. Exhib. Eur. Soc. Precis. Eng. Nanotechnol.*, 2017, pp. 149–150.
[8] S. Viëtor, "Tunable magnets: Modeling and validation for dynamic and precision applications," Master's thesis, Delft Univ. Technol., Delft, The Netherlands, 2018.
[9] R. Meijer, "Tunable magnets: Dynamic flux-feedback compensation methods for improved magnetization state tuning performance and minor-loop magnetization state tuning for the validation and reduction of the break-even tuning interval," Master's thesis, Delft Univ. Technol., Delft, The Netherlands, 2021.

[10] S. Ito, B. Lindner, and G. Schitter, "Sample-tracking vibration isolation with hybrid reluctance actuators for inline metrology," *IFAC-PapersOnLine*, vol. 52, no. 15, pp. 537–542, Sep. 2019.

[11] G. Stadler, E. Csencsics, S. Ito, and G. Schitter, "High precision hybrid reluctance actuator with integrated orientation independent zero power gravity compensation," *IEEE Trans. Ind. Electron.*, vol. 69, no. 12, pp. 13296–13304, Dec. 2022.

[12] S. Ito, F. Cigarini, and G. Schitter, "Flux-controlled hybrid reluctance actuator for high-precision scanning motion," *IEEE Trans. Ind. Electron.*, vol. 67, no. 11, pp. 9593–9600, Nov. 2019.

[13] E. P. Furlani, *Permanent Magnet and Electromechanical Devices: Materials, Analysis, and Applications*. San Diego, CA, USA: Acad. Press, 2001.

[14] I. R. I. MacKenzie, "Design and control methods for high-accuracy variable reluctance actuators," Ph.D. dissertation, Massachusetts Inst. Technol., Cambridge, MA, USA, 2015.

[15] W. Hoekwater, "Hybrid tunable magnet actuator: Design of a linearized force-flux tunable magnet actuator," Master's thesis, Delft Univ. Technol., Delft, The Netherlands, 2022.

[16] P. Campbell and S. Al-Murshid, "A model of anisotropic alnico magnets for field computation," *IEEE Trans. Magn.*, vol. 18, no. 3, pp. 898–904, May 1982.

[17] Eclipse Magnets, *Alnico Magnets Datasheet*, 2017. [Online]. Available: https://surfdrive.surf.nl/files/index.php/s/jjU4vuUqq1e0Sfq

[18] J. R. Brauer, *Magnetic Actuators and Sensors*. Hoboken, NJ, USA: Wiley-IEEE Press, 2006.

[19] HKCM Engineering, *Magnet-Cuboid Q10x10x20Nb-N48 Datasheet*, 2022. [Online]. Available: https://surfdrive.surf.nl/files/index.php/s/GfPzMkB1cmBSq3W

Endre Ronaes received the M.Sc. degree (cum laude) in mechanical engineering, with a specialization in mechatronic system design, in 2023 from TU Delft, Delft, The Netherlands, where he is currently working toward the Ph.D. degree in design and control of a low heat dissipation precision electromagnetic actuator with the Department of Precision and Microsystems Engineering.

His research focuses on the design of zero-heat dissipation electromagnetic actuators.

Hassan HosseinNia (Senior Member, IEEE) received the Ph.D. degree (cum laude) in electrical engineering from University of Extremadura, Spain, with a specialization in automatic control: application in mechatronics, in 2013.

He has an industrial background working at ABB, Västerås, Sweden. He is currently an Associate Professor with the Department of Precision and Microsystem Engineering, TU Delft, Delft, The Netherlands. He has (co)authored more than 100 publications in journals, conference proceedings, and book chapters. His research interests include precision mechatronic system design, precision motion control, and mechatronic systems with distributed actuation and sensing.

Dr. HosseinNia was the General Chair of the 7th IEEE international Conference in Control, Mechatronics and Automation (ICCMA 2019). He is also on the Editorial Board of the following four journals: *Fractional Calculus and Applied Analysis, Frontiers in Control Engineering, International Journal of Advanced Robotic Systems* (SAGE), and *Mathematical Problems in Engineering*.

William B. Hoekwater received the M.Sc. degree (cum laude) in mechanical engineering, with a specification in mechatronic system design, from the Technical University of Delft, Delft, The Netherlands, in 2022.

He is currently a Software Engineer with TTA, Bleskenschraaf, The Netherlands.